JOURNAL OF GEOPHYSICAL RESEARCH, VOL. 112, C09005, doi:10.1029/2007JC004105, 2007

The degree of anisotropy for mid-ocean currents from satellite observations and an eddy-permitting model simulation

Huei-Ping Huang,[1] Alexey Kaplan,[1] Enrique N. Curchitser,[2] and Nikolai A. Maximenko[3]

Received 16 January 2007; revised 30 April 2007; accepted 19 June 2007; published 12 September 2007.

[1] The degree of anisotropy is calculated for the mid-ocean currents estimated from satellite altimetry and simulated with a numerical model of the Pacific Ocean. A high resolution eddy-permitting model is used for its ability to simulate mid-ocean multiple zonal flows, crucial for the evaluation of the degree of anisotropy. Using a commonly defined parameter of anisotropy, α, that falls between -1 and 1 and equals 0, -1, and 1 for an isotropic, purely meridional, and purely zonal flow, respectively, it is found that α increases from nearly zero for weekly data to significantly positive values for seasonally and annually averaged data. This tendency of increasing zonal anisotropy with averaging time is true for the surface geostrophic velocity from satellite altimetry and for both surface and deep-ocean velocities from the model simulation. The absolute value of α for the simulated surface currents agree with that derived from satellite observation, reaffirming the reliability of both data sets. In the model simulation, the behavior of α at the surface is very similar to that at 1000 m, indicating a deep structure of the zonally elongated features in the middle of the Pacific Ocean. The implications of these findings are discussed in the context of oceanic eddies, Rossby waves, and zonal jets.

Citation: Huang, H.-P., A. Kaplan, E. N. Curchitser, and N. A. Maximenko (2007), The degree of anisotropy for mid-ocean currents from satellite observations and an eddy-permitting model simulation, *J. Geophys. Res.*, *112*, C09005, doi:10.1029/2007JC004105.

1. Introduction

[2] In the last decade the analyses of high-resolution satellite data have greatly enhanced our knowledge about the spatiotemporal structure of sea surface currents. Using a global data set from satellite altimetry, *Maximenko et al.* [2005] showed that the geostrophic currents derived from the observed sea surface height exhibit multiple zonal-jet structures upon time averaging, consistent with recent discoveries of mid-ocean jets in eddy-permitting ocean model simulations [*Nakano and Hasumi*, 2005; *Richards et al.*, 2006]. These recent findings raise many interesting questions, the most basic of which concerns the realism and robustness of the multiple zonal ‘‘stripes’’ in the velocity field. In recent studies the discussion on mid-ocean jets is often based on the map of the zonal component of the velocity, u, or that of the geostrophic velocity, u_g. Given that u_g is proportional to the meridional derivative of sea surface height (SSH), h, a random isotropic field of h could already correspond to east-west banded structures in u_g even when no real zonal jets exist. In this case, the meridional geostrophic velocity, v_g, would exhibit north-south stripes since v_g is proportional to the zonal derivative of h. (See appendix A.) The flow field is not truly zonally anisotropic if the north-south stripes in v_g are as strong as the east-west stripes in u_g. There is indeed a hint of this situation in a typical example, shown in Figure 1, of a set of weekly fields of u_g and v_g over the North Pacific derived from satellite altimetry (detail in section 2). Figure 2 is similar to Figure 1 but for 50-week averaged fields of u_g and v_g. Here, after substantial time averaging, the east-west stripes in u_g become much stronger than the (still visible) north-south stripes in v_g, indicating that zonal anisotropy is real on the 50-week timescale. (Alternatively, one can also show that the zonal jets are real by demonstrating their existence in the vorticity field, as did *Maximenko et al.* [2005]. In this study we choose to analyze the velocity field as the vorticity field is noisier and not ideal for a visual comparison of the observations and the model simulation.)

[3] The examples in Figures 1 and 2 suggest two points for investigations. First, to solidify the claims made in recent studies of the dominance of multiple zonal flows in the mid-ocean, it is useful to consider both u and v components and quantify the degree of anisotropy of the velocity field. Secondly, the degree of anisotropy and the zonal-jet structure of the flow field clearly depends on time averaging. For example, *Maximenko et al.* [2005] suggested that time averaging of westward drifting eddies may lead to a visually zonal-jet like structure. Thus the timescale at which zonal anisotropy emerges may provide a useful hint for the

[1]Lamont-Doherty Earth Observatory of Columbia University, Palisades, New York, USA.
[2]Institute of Marine and Coastal Sciences, Rutgers University, New Brunswick, New Jersey, USA.
[3]International Pacific Research Center, SOEST, University of Hawaii at Manoa, Honolulu, Hawaii, USA.

0148-0227/07/2007JC004105$09.00

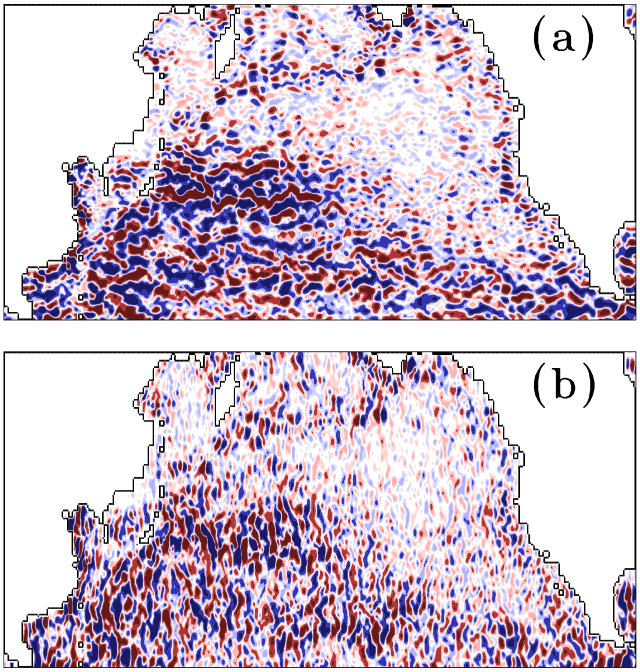

Figure 1. (a) A randomly selected weekly map of the zonal component of the surface geostrophic velocity derived from AVISO altimetry SSH anomaly. (b) Same as (a) but for the meridional component. Color scales are ±2, 4, 8, 16 cm s^{-1} with red and blue indicating positive and negative values, respectively.

dynamics of the zonally coherent structures. Anticipating future investigations in this direction, in this study we will perform straightforward calculations of the degree of anisotropy for the velocity field as a function of the length of time averaging for both observations and a numerical simulation.

[4] Observations from satellite altimetry and a simulation based on an eddy-permitting model for the Pacific are used in this study. Although sparse in situ observations exist for the surface and deep ocean currents, we choose the altimetry data for its extensive and uniform spatial-temporal coverage at high resolution that are needed for our calculation. Satellite data only provide information for the surface. They are complemented by the ocean model simulation that produces both surface and deep ocean currents. A cross-validation of the simulated and observed currents at the surface will help reassure the reliability of both data sources. The model used here is eddy-permitting, guided by results from recent studies that mid-ocean multiple zonal flows emerge only after the model properly resolves meso-scale eddies [*Treguier et al.*, 2003; *Nakano and Hasumi*, 2005]. The degree of anisotropy provides a simple measure of the "zonality" of the flow field, ideal for a first quantitative analysis and comparison of the strength of zonal currents in observations and simulations. Considerations of more complicated statistics, e.g., those that measure the sharpness or curvature of the profile of zonal velocity, are left for future work. In the following, section 2 is devoted to the calculations for the degree of anisotropy for the altimetry data. Section 3 repeats these calculations for the numerical simulation. Discussion and concluding remarks follow in sections 4 and 5.

2. Satellite Observation

2.1. The Altimetry Data

[5] The data used here is from the processed AVISO altimetry measurements for SSH [*Ducet et al.*, 2000]. It has 1/3-degree Mercator resolution in space and is archived as weekly means. Since the AVISO data was processed with a mapping function with a 15-day timescale, it is understood that the "weekly fields" in this paper are in fact temporally smoothed with an effective resolution slightly longer than a week. The coverage of the data is global but for our purpose it suffices to focus on the North Pacific.

[6] The surface geostrophic velocities, (u_g, v_g), are derived from SSH by the geostrophic relationship, taking into account spherical geometry. A local fourth order finite difference scheme [e.g., *Castillo et al.*, 1995] is used. Since geostrophic relationship breaks down in the lower latitudes and since the Tropics has its own distinctive current system, only the domain north of 12°N (the entire domain shown in Figure 1) is considered. The weekly data consists of 639 records spanning about 12 years. Guided by Figures 1 and 2, N-week averaged data sets (based on non-overlapping N-week segments, e.g., there are 127 such segments for N = 5) are constructed from the weekly data, with selected values of N = 1, 5, 10, 20, 50, and 100. (N = 1 corresponds to the "unaveraged" weekly data.)

[7] The altimetry data used here is the anomaly relative to the long-term (1992–2002) mean. The long-term mean of the altimetry SSH includes geoid that is unrelated to geostrophic ocean currents. The construction of the absolute

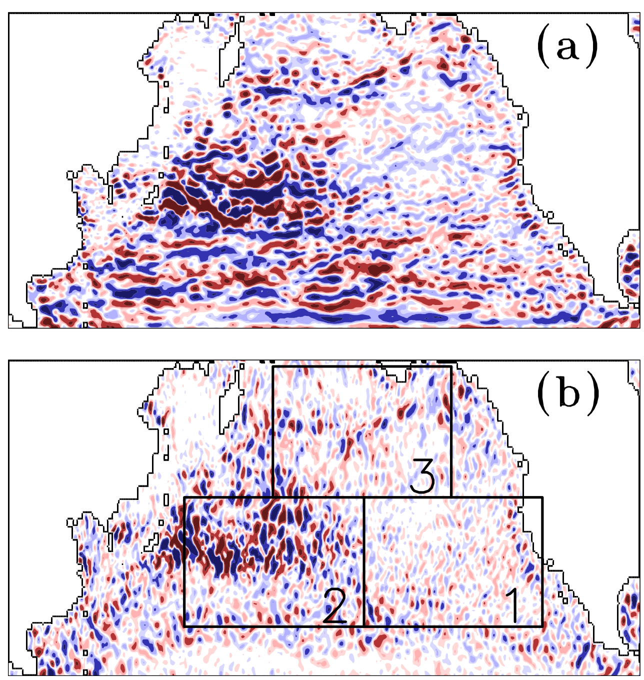

Figure 2. Same as Figure 1 but for a randomly selected 50-week averaged surface geostrophic velocity field. (a) Zonal component. (b) Meridional component. The color scales are ±1, 2, 4, 8 cm s^{-1}.

dynamic topography based on different combinations of satellite and in situ data is by itself a complicated issue [e.g., *Tapley et al.*, 2003; *Maximenko and Niiler*, 2005; *Jayne*, 2006]. We will first focus on the anomalous SSH in the analysis of the satellite data, deferring a discussion on the absolute velocity to later sections.

[8] In addition to the long-term mean, the mean seasonal cycle, defined as the sum of the averaged annual and semiannual harmonics, is also removed from the SSH in our major calculations for both satellite observations and the model simulation. We have tested selected cases to ensure that the removal or addition of the seasonal harmonics does not affect our conclusions.

2.2. Degree of Anisotropy

[9] The degree of anisotropy of the horizontal velocity for a given spatial domain is defined by

$$\alpha = \frac{\langle u^2 \rangle - \langle v^2 \rangle}{\langle u^2 \rangle + \langle v^2 \rangle}, \tag{1}$$

where $\langle u^2 \rangle$ indicates the area-weighted domain average of u^2. The domain averaged velocity is removed before the calculation of the variance. For the satellite data, geostrophic velocities (u_g, v_g) are used in the places of (u, v) in (1). The definition in (1) is standard and has been used elsewhere for the studies of quasi two dimensional flows [e.g., *Shepherd*, 1990]. Note that $-1 \leq \alpha \leq 1$ and $\alpha = 0$, -1, and 1 for an isotropic, purely meridional (north-south), and purely zonal (east-west) flow, respectively. The value of α is connected to the horizontal aspect ratio of the disturbances in the flow field. Consider for instance a disturbance with $\psi \sim \exp[i(k_x x + k_y y)]$ in a non-divergent flow where ψ is the stream function and $k_x = 2\pi/L_x$ and $k_y = 2\pi/L_y$ are horizontal wave numbers. Using the relation, $(u, v) = (-\partial\psi/\partial y, \partial\psi/\partial x)$, and (1) we obtain

$$\alpha = \frac{L_x^2 - L_y^2}{L_x^2 + L_y^2} \tag{2}$$

Thus $\alpha \to 1$ when $L_x \gg L_y$, and $\alpha \to -1$ when $L_x \ll L_y$.

[10] The values of α are calculated for the whole North Pacific (north of 12°N) domain and for several of its subdomains, shown in Figure 2b as the boxes. They include Box 1 in the Eastern Pacific far away from the western boundary currents (but including some eastern boundary currents), Box 2 to its west that contains some of the extensions of the western boundary currents, and Box 3 in the far North Pacific, an area that includes significantly non-zonal bottom topography and boundary currents.

[11] Figure 3 shows the value of α for the four named domains as a function of N, the number of weeks over which time averaging is performed. The filled circles are the mean. For example, for N = 5 it is the average over 127 values of α each calculated with equation (1), with the u_g and v_g in the equation being the 5-week means. The vertical bar indicates ±1 standard deviation. (The vertical bar for N = 100 might be less reliable since it is deduced from only 6 records.) Two important features emerge. First, except for Box 3, the unaveraged weekly surface geostrophic current is nearly isotropic with $\alpha \approx 0$. This confirms our first impression of Figure 1 as described in section 1. Second, α clearly increases toward positive zonal anisotropy with time averaging. This tendency is true for all domains. The typical value of α is between 0.3 and 0.5 under a 1-year average depending on the location. The lower value of α for Box 3 may be due to the permanent anisotropic signatures in the flow in that region associated with the Aleutian boundary current. Note as well that in the higher latitudes the eddies are generally smaller due to a larger Coriolis parameter and, hence, a smaller deformation

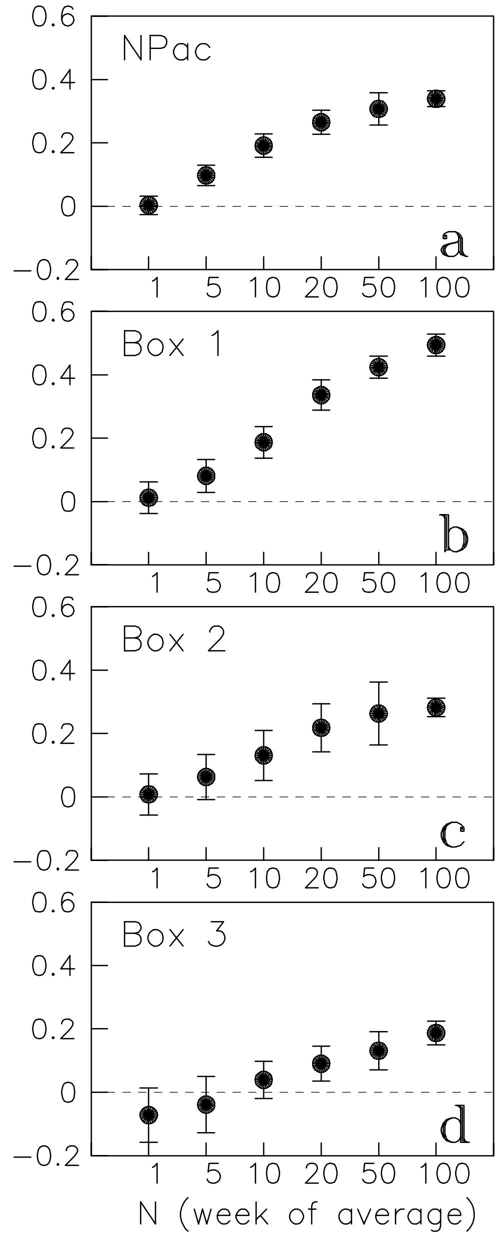

Figure 3. The degree of anisotropy, α, calculated from the surface geostrophic velocity field for (a) The North Pacific, (b) Box 1, (c) Box 2, and (d) Box 3. The geostrophic velocity is derived from altimetry SSH. The numbers on the abscissa indicate that the statistics of α are constructed from 1-week, 5-week, . . ., 100-week averaged data. The circles and vertical sticks are mean and standard deviation.

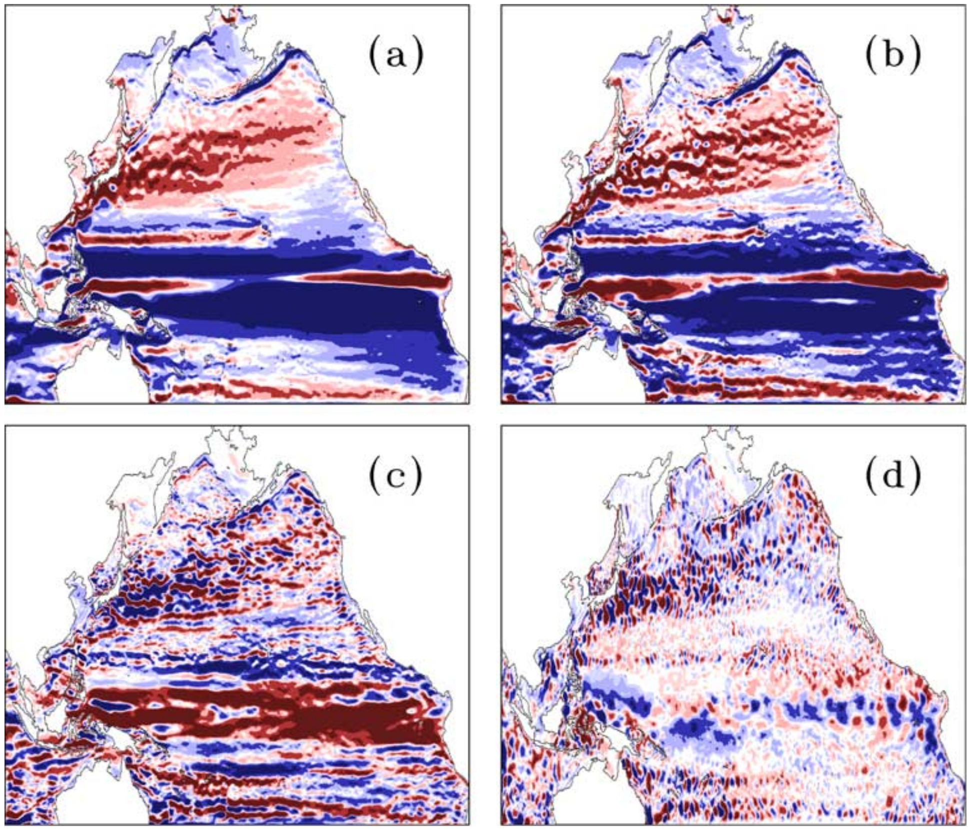

Figure 4. The velocity fields from the ocean model simulation. (a) The long-term (12-year) mean of the surface zonal velocity. (b) A selected 1-year (last year of a 20-year run) mean of the surface zonal velocity. (c) The 1-year average of the anomalous surface zonal velocity, defined as (b) minus (a). (d) Same as (c) but for the surface meridional velocity. Color scales are ±2, 4, 8, 16 cm s^{-1} for (a) and (b) and ±1, 2, 4, 8 cm s^{-1} for (c) and (d). Red and blue colors indicate positive and negative values, respectively.

radius [*Chelton et al.*, 1998]. They might be relatively poorly resolved by altimetry [e.g., *Pascual et al.*, 2006]. The largest (positive) values of α are found in Box 1, far away from the influences of the western boundary currents.

3. Ocean Model Simulation

3.1. The Model

[12] The ROMS (Regional Ocean Modeling System) model [*Curchitser et al.*, 2005; *Shchepetkin and McWilliams*, 2005] is used for the eddy-permitting simulation of the Pacific Ocean. It has a flexible horizontal grid system and terrain-following vertical levels. This study uses a new run with a 0.18 degree horizontal resolution and 42 terrain-following levels. An illustration of the model levels and detail of the bathymetry are given in Appendix B. The model domain extends from 30S to 65N, and from 90E to 290E. The surface forcing is derived from the CORE data set [*Large and Yeager*, 2004]. The high-resolution North Pacific model is nested within a 1 degree global ocean hindcast simulation using the National Center for Atmospheric Research (NCAR) Community Climate System Model (CCSM). The initial conditions are derived from a fully evolved ocean model so that a relatively short period of adjustment is needed. For the comparison with altimetry data, we will focus on the North Pacific domain between 12N and 60N. The model outputs from the last 12 years, comparable in length to the satellite data, of a 20-year run will be used. Unlike the satellite data, the model simulation produces a straightforward long-term mean of the velocity field. For a comparison with satellite data we will first analyze the anomalies but will restore the long-term mean in a later discussion.

[13] Figure 4 shows the model simulated surface velocity. (Hereafter, the velocity from the model refers to the full velocity, not geostrophic velocity derived from the SSH field as in the satellite data.) Figure 4a is the long-term (12-year) mean of u, Figure 4b shows a selected one-year mean of u, and Figure 4c is the one-year mean of the anomaly of u, defined as Figure 4b minus Figure 4a. Figure 4d is similar to Figure 4c but for the meridional velocity, v. Now Figures 4c and 4d can be compared with the 50-week averaged geostrophic velocity in the satellite data in Figures 2a and 2b. They contain similar features, with the east-west stripes in u much stronger than the north-south stripes in v, indicating the dominance of zonal velocity under the annual average. The magnitude of the simulated surface velocity is also similar to its counterpart

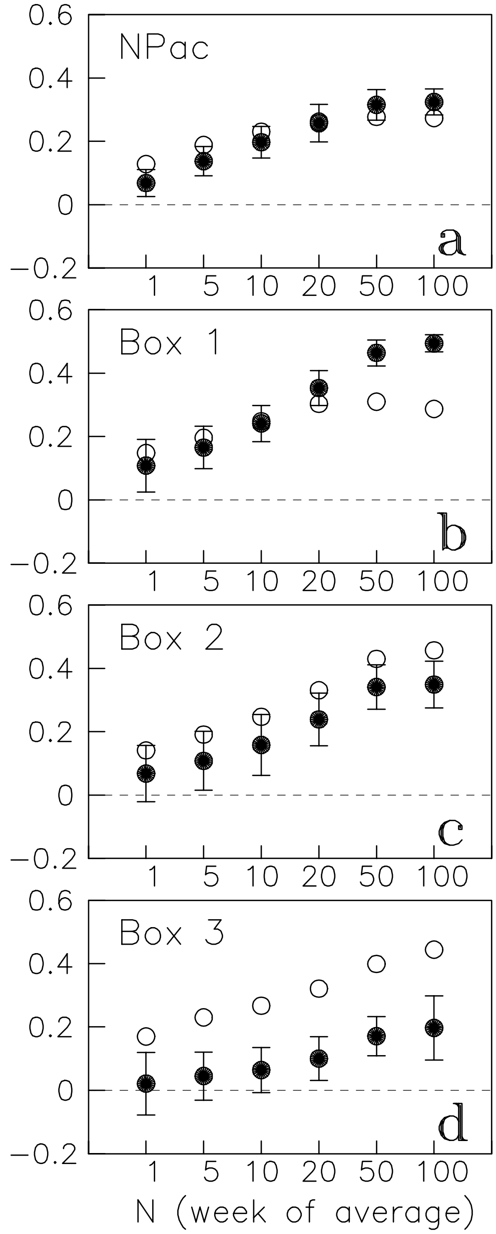

Figure 5. The filled circles and error bars are same as Figure 3 but are for the statistics of α derived from the surface velocity in the model simulation. The open circles are counterparts of the filled circles with the long-term mean included in the velocity field in the calculations of α (see section 3.5).

in satellite data. Note that the east-west stripes in *u* are also visible in the one-year mean in Figure 4b and even the long-term mean in Figure 4a, although they are not as prominent as those in the anomaly field in Figure 4c.

3.2. Degree of Anisotropy at the Surface

[14] We first evaluate α for the simulated anomalous surface velocity for a direct comparison with the satellite observations. The statistics of α, the counterparts of Figure 3 for the model simulation, are shown in Figure 5. As before, the filled circle and vertical bar are the mean and standard deviation of α calculated from the anomalous velocity field. Because the model outputs were archived as four-day means, the previously used 1, 5, 10, 20, 50, and 100 weeks of time averaging are approximated as 8, 36, 72, 140, 348, and 700 days, respectively, for the model data. For simplicity we retain the notations in Figure 3. Figure 5 agrees with Figure 3 in the overall values of α and their tendency to increase with time averaging. The agreement extends to individual subdomains of the North Pacific. For example, Box 1 in the Eastern Pacific has the highest values of α, while Box 3 has the lowest values with α being slightly negative at N = 1. In both model and satellite data, over the North Pacific and Boxes 1 and 2, α is close to zero for N = 1, confirming that the unaveraged weekly velocity field is nearly isotropic.

[15] In the above calculation we have used the full velocity because it can be readily compared with the simulated velocity fields in the deep ocean. Since the scales of the zonal jets of our interest mostly fall within the range in which geostrophic approximation is valid, our main results concerning the degree of anisotropy remain very similar if the surface velocity field is replaced with the surface geostrophic velocity field derived from the simulated SSH. This is demonstrated in Appendix C.

3.3. Degree of Anisotropy at 1000 m

[16] The model simulation provides additional information of the flow fields in the deep ocean. Figure 6 shows the counterparts of Figure 4 for the model-simulated velocity at 1000 m. The east-west stripes in *u* are even more prominent in the deep ocean compared to those at the surface. The zonal bands are clearly visible not only in the anomaly field (Figure 6c) but also in the total *u* field (Figure 6b) with one-year averaging. These are consistent with other recent eddy-permitting simulations of the Pacific and other ocean basins using different models [*Nakano and Hasumi*, 2005; *Maximenko et al.*, 2005; *Richards et al.*, 2006; *Treguier et al.*, 2003] In the long-term mean (Figure 6a), the multiple zonal bands are relatively weaker in the North Pacific but they remain visible. A comparison of Figures 6c (*u* velocity) and 6d (*v* velocity) indicates that the flow in the mid-ocean is dominated by the zonal velocity. This may justify the focus on the *u* velocity in identifying the deep ocean zonal-jet structure in previous modeling studies [*Nakano and Hasumi*, 2005; *Richards et al.*, 2006].

[17] Figure 7 shows the values of α for the simulated velocity at 1000 m in the same format as Figure 5. The behavior of α in the deep ocean is similar to that at the surface. Again, α increases with time averaging, with its highest values associated with Box 1 and lowest values with Box 3. Except for Box 3, the values of α at 1000 m generally exceed those at the surface. Notably, for the North Pacific and Boxes 1 and 2, α is already positive even for N = 1 (the weekly data).

3.4. The Tropics

[18] We have so far excluded the Tropics from our discussion, partly to circumvent the inaccuracy in the geostrophic velocity derived from the satellite-observed SSH but also due to the consideration that the zonal currents in the Tropical ocean are governed by dynamics different from that governing the extratropical mid-ocean currents of our interest. Nevertheless, since east-west stripes in *u* are

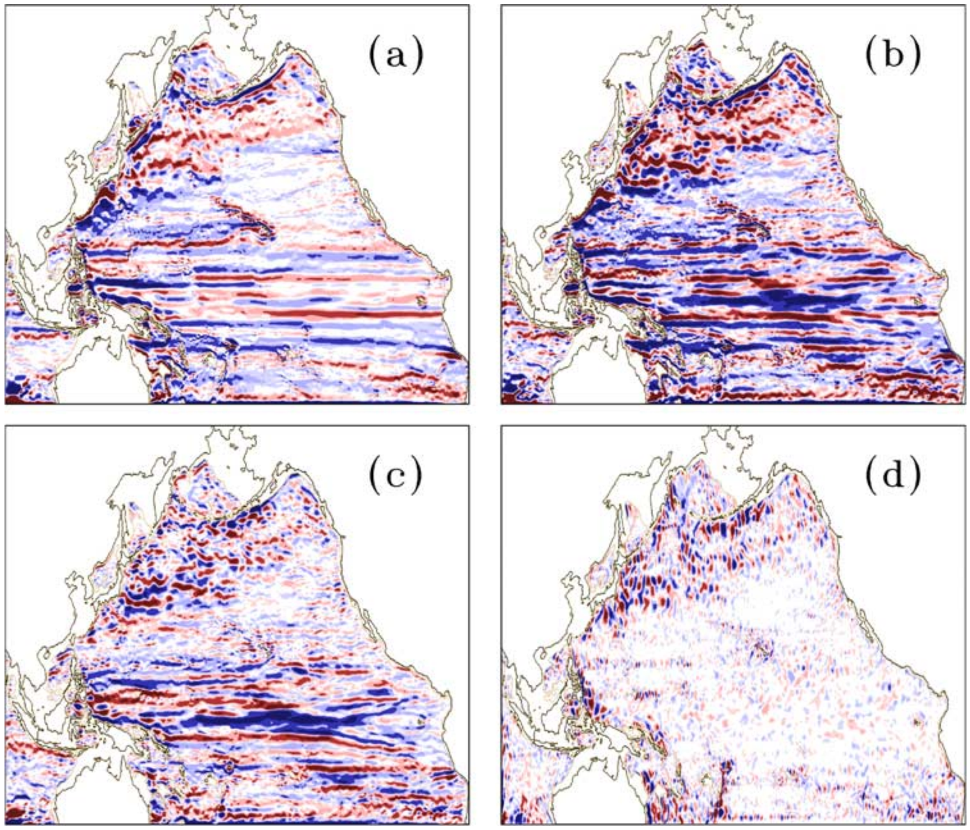

Figure 6. Same as Figure 4 but for the model simulated velocity fields at 1000 m. (a) Long-term mean of *u*. (b) One-year average of *u*. (c) One-year average of the anomaly of *u*, defined as (b) minus (a). The period chosen for (b) and (c) is the same as that for Figure 4c. (d) Same as (c) but for the *v* component. Color scales are ±0.5, 1, 2, 4 cm s^{-1} for all panels. Red and blue indicate positive and negative values, respectively.

clearly visible at low latitudes in the model simulation, for completeness of this work, α is calculated from the simulated velocity at the surface and at 1000 m as shown in Figure 8. Here, the Tropical region is defined as the latitude belt between 18N and 18S. Large positive values of α are found both at 1000 m and at the surface. They are greater than those for the midlatitude shown in Figures 5 and 7.

3.5. The Long-Term Mean

[19] The preceding discussions have excluded the long-term mean of the velocity field. With the satellite data, the determination of the absolute dynamic topography is nontrivial because the time-mean SSH from altimetry contains elements (geoid, tides) that are unrelated to geostrophic ocean currents. Recently, attempts have been made to construct the long-term mean absolute dynamic topography from different combinations of altimetry, GRACE, and in situ observations [e.g., *Tapley et al.*, 2003; *Maximenko and Niiler*, 2005; *Jayne*, 2006]. The geostrophic *u*-velocity derived from a 10-year (1992–2002) mean of the absolute dynamic topography with 0.5° resolution from *Maximenko and Niiler* [2005], which combines all of the altimetry, GRACE, NCEP wind, and in situ drifter data, is shown in Figure 9. In the North Pacific, Figure 9 broadly resembles the simulated long-term mean of the surface *u*-velocity in Figure 4a, both in magnitude and in large-scale pattern. At the finer scales, there is a hint of multiple zonal bands in the observation but they are not as prominent as those in the model simulation.

[20] Unlike the observation, the ocean model simulation produces a straightforward time-mean velocity field as shown in Figures 4a and 6a. Adding the time mean back to the anomaly fields, the statistics of α for the total velocity at the surface and 1000 m are calculated for the North Pacific as shown in Figures 5a–5d and 7a–7d in open circles. In general, up to N = 50, the tendency for α to increase with time averaging remains similar with or without the time mean. The error bars for the open circles (not shown) are also comparable to their counterparts for the filled circles.

4. Discussion

[21] We have shown that a 20-to-50 week average generally leads to significantly positive zonal anisotropy of the velocity field at both surface and 1000 m. This finding supports the uses of 18-week to multiyear averaged *u* field in identifying the mid-ocean zonal jets in recent observational and modeling studies [*Maximenko et al.*, 2005; *Richards et al.*, 2006]. The unaveraged velocity field is found to be nearly isotropic. This may reflect the direct influences of high-frequency random atmospheric forcing. Notably, at the weekly timescale, the velocity at the surface is especially

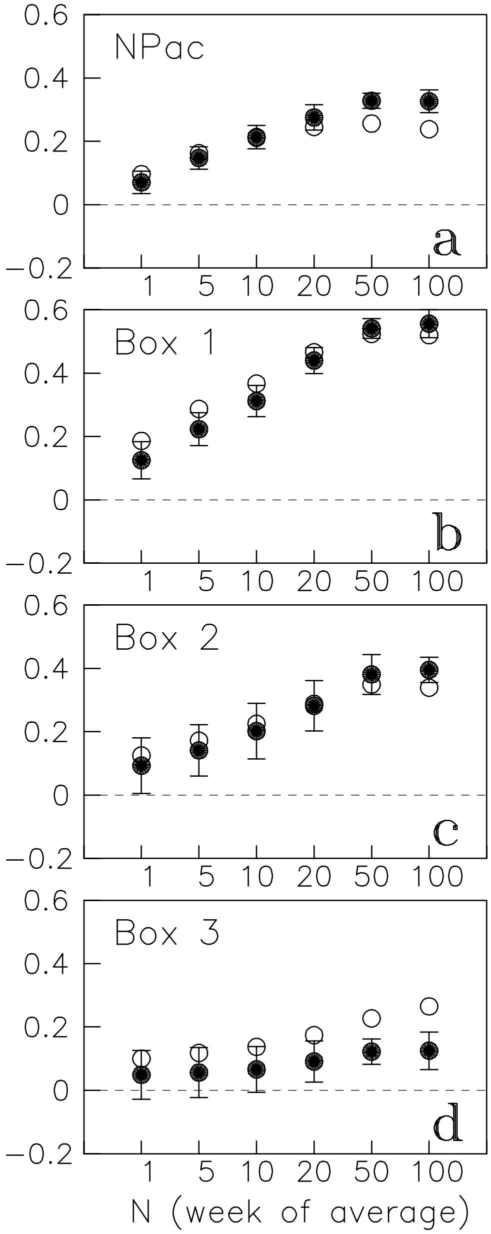

Figure 7. Same as Figure 5 but for the statistics of α derived from the model simulated velocity at 1000 m.

close to isotropy while that at 1000 m – away from the atmospheric influence – is slightly zonally anisotropic.

[22] The timescale we found on which zonal anisotropy emerges is also consistent with an early analysis by *Cox* [1987], who considered the structure of the stream function (equivalent to our use of both u and v components) simulated by an idealized eddy-permitting model. The temporally unfiltered stream function field is nearly isotropic, while strongly zonal anisotropy emerges under a temporal low-pass filter with a decorrelation scale of about a half year [see *Cox*, 1987, Figures 12 and 13].

[23] A deeper understanding of the behavior of α depicted in Figures 3–7 would require detailed studies based on the dynamical properties of the oceanic eddies/waves and jets. To stimulate future research, a few (not all-inclusive) scenarios are outlined in the following.

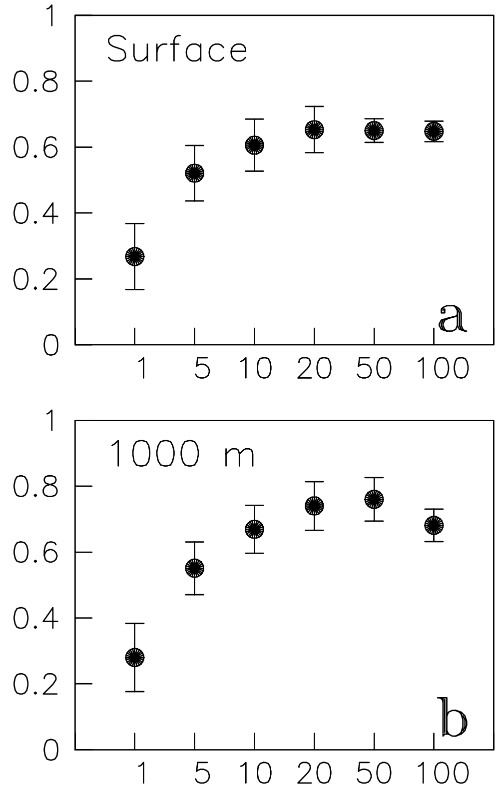

Figure 8. Same as Figures 3 and 5 but for the statistics of α for the simulated velocity in the Tropics (between 18N and 18S). (a) Surface. (b) 1000 m.

4.1. Time Averaging of Longitudinally Drifting Eddies

[24] *Maximenko et al.* [2005] have previously noted that averaging a westward drifting eddy over time may produce a visually jet-streak like structure, corresponding to a

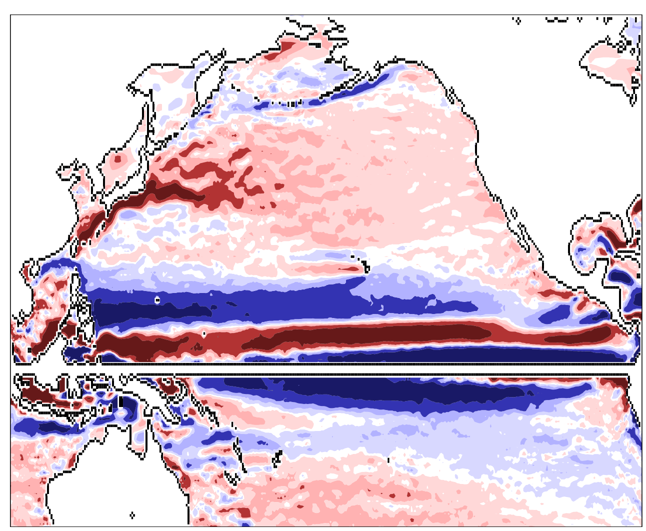

Figure 9. The zonal component of the surface geostrophic velocity derived from the 10-year mean absolute dynamic topography of *Maximenko and Niiler* [2005]. Color scales are ±1, 4, 8, 16 cm s^{-1}. Red and blue indicate positive and negative values, respectively.

positive α. However, they also found that the characteristic length scale of an observed zonal jet streak generally exceeds that of the expected displacement of the eddies [*Chelton and Schlax*, 1996]. For the current discussion, it is interesting to derive α as a function of the averaging time, T, from a simple setting that mimics a field of drifting eddies.

[25] Assuming a constant east-west drifting velocity, U, and an initially isotropic field of eddies with a spatial scale $L_x = L_y = R$. Averaging over time, L_y remains unchanged but the drifting leads to $L_x = R + UT$. Using equation (2), one obtains

$$\alpha = \frac{1 - (1 + \gamma T)^{-2}}{1 + (1 + \gamma T)^{-2}} \tag{3}$$

where $\gamma = U/R$ is a constant. For example, choosing R = 50 km (typical for the mesoscale eddies) and U = 1 cm/s gives γ^{-1} ~8 weeks. Figure 10a shows selected curves of α (T) with γ^{-1} = 8, 16, 32, and 64 weeks. Qualitatively, these curves exhibit some of the characteristics of the observed α, with $\alpha = 0$ at $T = 0$ and α increases with T. However, superimposing over these curves the values of α from the observation and ocean model simulation (symbols in Figure 10a) does not reveal a good fit of the data. The goodness of fit can also be measured by the extent that γ remains a constant (independent of T) for the observed or simulated data. Using the relation

$$\gamma = T^{-1}\left[\left(\frac{1+\alpha}{1-\alpha}\right)^{1/2} - 1\right] \tag{4}$$

derived from equation (3), the values of $\gamma(T)$ for selected data from Figures 3–7 are plotted in Figure 10b. They do not remain constant but vary by an order of magnitude for the range of T from 0 to 100 weeks.

[26] This example only considers the simplest setting, with a strictly east-west drift velocity (ignoring the expected slight north-south drift and the cyclone-anticyclone asymmetry, *Morrow et al.* [2004]; *Chelton et al.* [2006]) and a fixed shape of the eddies as they drift. Nevertheless, it illustrates that it is not trivial to explain the zonal anisotropy by considering only a simple drift of the eddies. More complicated mechanisms may be needed to quantitatively explain the observed and simulated jet streaks.

4.2. The Non-Isotropic Dispersion Relation of Rossby Waves

[27] In contrast to the "drifting eddy" point of view, one may consider another limit when the ocean is occupied by approximately linear waves that preserve their dispersion relation. The linear wave thinking is often adopted for studying the large-scale disturbances in the atmosphere. To draw an analogy, note that a similar behavior of an increasing α with T is known for the synoptic and low-frequency variability in the atmosphere. High-frequency (e.g.,$T \sim 1$ week) disturbances tend to be meridionally elongated while low-frequency (e.g., $T > 1$ month) ones are zonally elongated [*Wallace and Lau*, 1985]. Because large-scale, low-frequency disturbances in the atmosphere are dominated by Rossby waves and are nearly barotropic, one could possibly interpret this behavior as a consequence of the dispersion relation of the barotropic Rossby wave modes, $\omega_{\mathbf{k}} = -\beta k_x/(k_x^2 + k_y^2)$, where $\omega_{\mathbf{k}}$ is the frequency of the **k**-th mode, $\mathbf{k} = (k_x, k_y)$ is the wave number vector, and β is the meridional gradient of the Coriolis parameter, f. For a given total wave number, $K = (k_x^2 + k_y^2)^{1/2}$, zonally elongated disturbances ($k_x < k_y$, a special case is the zonal mean flow with $k_x = 0$) are more capable of surviving a low-pass temporal filter because they have lower frequencies. (For simplicity, we ignore the effect of the climatological mean flow on $\omega_{\mathbf{k}}$, which is important for the atmosphere, e.g., *Simmons et al.* [1983]). Thus the value of α for the wavefield increases after time averaging.

[28] The above argument relies on the fact that the dispersion relation of Rossby waves is non-isotropic, in

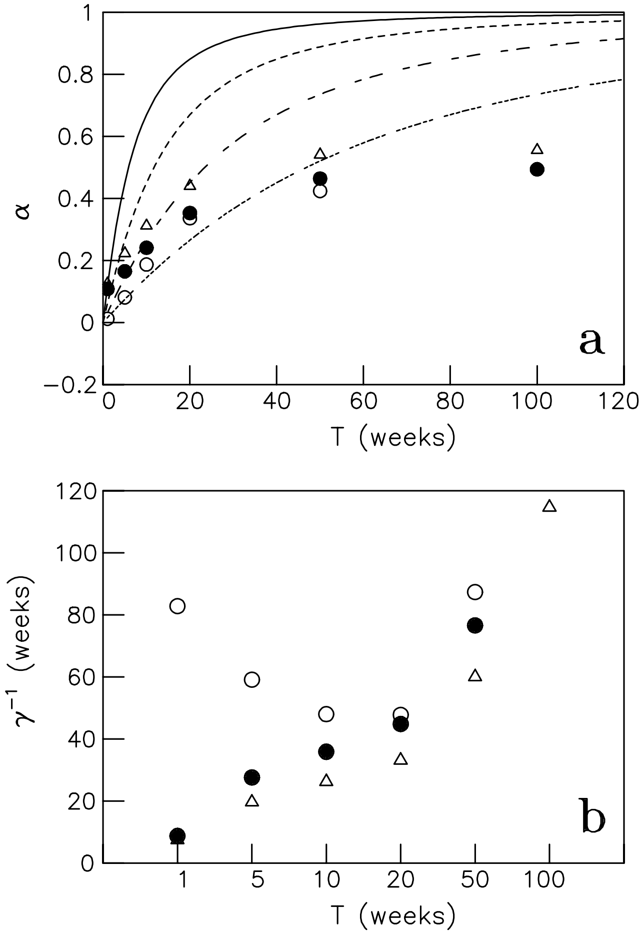

Figure 10. (a) Selected curves of α as a function of T plotted in linear scale for (top to bottom) γ^{-1} = 8, 16, 32, and 64 weeks based on equation (3). The symbols are the observed and simulated values of α for the Box 1 region from Figures 3b (open circle), 5b (filled circle), and 7b (triangle). (The filled circle almost coincide with open circle at T = 100.) (b) The values of γ^{-1} as a function of T using equation (4) and the observed and simulated values of α from Figures 3b, 5b, and 7b. The symbols used here correspond to their counterparts in (a).

the sense that $\omega_{\mathbf{k}}$ is not invariant under a swapping of k_x and k_y. Quantitatively, it is complicated to test this idea for the ocean, due to the presence therein of many different wave modes (barotropic and baroclinic Rossby, gravity, etc.) that possess different dispersion relations. As a pedagogical example, in Appendix D we illustrate the increase of α with T for a random wavefield that consists of only the barotropic Rossby wave modes. In that model, the value of α at large T turns out to be not unreasonable compared to the observation, although the behavior of α at small T is less realistic and the value of α is found to be somewhat sensitive to the choice of the prescribed energy spectrum of the unaveraged wavefield.

4.3. Dynamical Pictures and Beyond

[29] The scenarios discussed above represent the two limits of idealization (eddies that preserve their shape vs. waves that preserve their dispersion relation). The real world is likely located somewhere in between. Nevertheless, the simple examples serve to illustrate that, in principle, a theory for the mid-ocean currents or eddies/waves should be able to predict the behavior of α, which can then be verified with those obtained from the observations or comprehensive model simulations.

[30] The simple models discussed in sections 4.1 and 4.2 are kinematic, disregarding how the ensemble of waves or eddies are generated or how they interact among themselves. A more comprehensive theory should ultimately include this aspect by incorporating relevant dynamical processes for the eddies and waves. An example of such processes is the upscale energy cascade in geostrophic turbulence [e.g., *Smith and Vallis*, 2001; *Galperin et al.*, 2004; *Scott and Wang*, 2005 for recent discussions] that takes place between the Rossby radius of deformation, $L_R \sim 50$ km, where the mesoscale eddies are generated, and Rhines scale, $L_\beta \sim$ a few hundred km, that coincides with the meridional scale of the jet streaks [*Rhines*, 1975, 1979]. While it is beyond our scope to test this dynamical picture, it is useful to note that, for Rossby wave turbulence, the triad interaction that forms the basis of the upscale energy cascade inherently implies a tendency toward zonal anisotropy by Hasselmann's lemma [see *Rhines*, 1975; *Fu and Flierl*, 1980; *Huang et al.*, 2001]. In short, it dictates that energy be transferred from high frequency to low-frequency modes but the latter have stronger zonal anisotropy for Rossby waves. Thus the values of α shown in Figures 3, 5, and 7 might also be used as a constraint to verify a proposed dynamical process for the formation of jet streaks in mid-ocean.

[31] Last, we note that several recent studies have also attempted to interpret the anisotropic property of the observed sea surface disturbances from different perspectives. *Maximenko and Niiler* [2006] noted that the mid-ocean jet streaks are not always strictly zonal but they often have a tilt. The tilted structure is interpreted as stationary Rossby waves standing in the large-scale background flow. (In the context of our analysis, stationary Rossby waves by definition will survive time averaging for any values of T.) *Logan et al.* [2006] and *Sen et al.* [2006] found practical isotropy in the weekly surface geostrophic velocity from altimetry but they also suggested the existence of persistent small-scale anisotropic structures in the flow field that are independent of time averaging. How to reconcile and unify all of the above point of views is a major task for future studies.

5. Concluding Remarks

[32] Our analysis of α provides a quantitative support for the claimed basin-wide "zonality" (dominance of zonal velocity in the flow field) in the surface and deep ocean currents based on 18-week to multiyear averaged u velocity [*Maximenko et al.*, 2005; *Richards et al.*, 2006]. On these timescales, the degree of anisotropy is found to be significantly positive and similar in value in both the surface velocity field from satellite altimetry and the surface and deep ocean velocity fields from an eddy-permitting model simulation. The unaveraged weekly velocity field is found to be nearly isotropic. The effect of low-pass temporal filtering is to remove meridionally elongated structures but spare or accentuate zonally elongated ones. The connection of this behavior with the property of Rossby waves (with or without a background mean flow) or that of a set of drifting eddies awaits further investigations.

[33] Our results also confirm, for the first time, the consistency in the anisotropic properties of the velocity fields between high-resolution satellite observations and an eddy-permitting ocean model simulation. These results raise our confidence in using the ocean model for future investigations of mid-ocean jets, whose basin-wide three-dimensional structures are difficult to observe by either conventional or satellite-based methodologies. Our analysis of the model output reveals very similar behaviors of α at the surface and at 1000 m, hinting at possibly a deep structure of the zonally anisotropic features in mid-ocean.

[34] The degree of anisotropy calculated in this study measures the zonality of the flow field regardless of the detailed profiles of the zonal velocity. Analyses of other refined measures, for instance one that detects the sharpness of the velocity profile (such a measure would have to depend on the gradient of the velocity), are useful next steps. Nevertheless, the simple definition of α here allows a quick calculation of its value for any flow field from observations, simulations, and theories. As a first test, we expect a viable theory for the mid-ocean zonal currents to be able to reproduce the behavior of α as shown in Figures 3, 5, and 7.

Appendix A: Some Kinematic Relationships Concerning Isotropy

[35] Consider a random isotropic field of SSH with $|h_{\mathbf{k}}|^2 \sim K^{-p}$, where $h_{\mathbf{k}}$ is the k-th Fourier component of h, $\mathbf{k} = (k_x, k_y)$ is the wave number vector, and $K = (k_x^2 + k_y^2)^{1/2}$ is the total wave number. (In the ensuing argument, K^{-p} can also be replaced by a more general function, $H(K)$, that depends only on the total wave number.) By using the geostrophic relation between u and h in spectral space, $u_{\mathbf{k}} \sim ik_y\, h_{\mathbf{k}}$, the "energy spectrum" for the u-component of geostrophic velocity becomes $|u_{\mathbf{k}}|^2 \sim k_y^2\, K^{-p}$, which is not isotropic but has more energy in the Fourier components with $|k_y| > |k_x|$ (those with a zonally elongated structure) than in those with $|k_x| > |k_y|$. The opposite is true for the v-component of the geostrophic velocity, with $|v_{\mathbf{k}}|^2 \sim k_x^2\, K^{-p}$. However, putting u

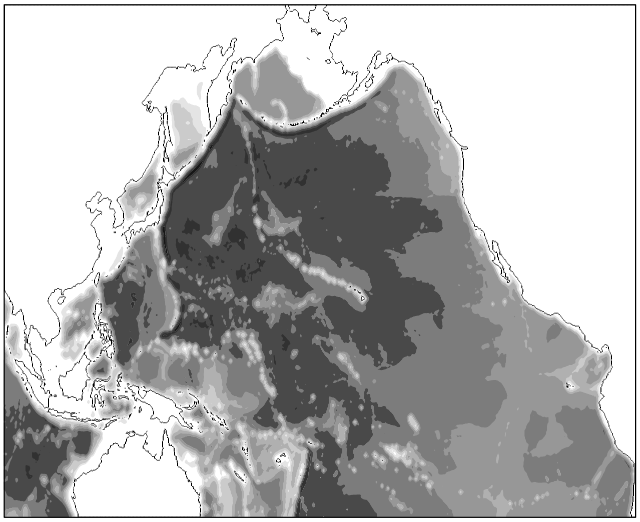

Figure B1. The model domain and bathymetry used for the ocean model simulation. The gray scales for depth are 0.5, 1, 2, 3, 4, 5, 6, 7 km. Areas that are shallower than 500 m are white.

and v together, the energy spectrum for the velocity vector field (u, v) is isotropic with $|u_{\mathbf{k}}|^2 + |v_{\mathbf{k}}|^2 \sim K^{-p+2}$. Similarly, the energy spectrum of the stream function or vorticity field constructed from the velocity vector is also isotropic.

Appendix B: ROMS Model Domain and Bathymetry

[36] The model domain for the Pacific run used in section 3 is shown in Figure B1. Although our analyses are focused on the North Pacific, the model covers part of the South Pacific and the entire Tropical Pacific. A realistic bathymetry is used, as also shown in Figure B1. Note that the choices of the bathymetry (realistic vs. flat-bottom) may affect the temporal behavior of the simulated zonally elongated structures in mid-ocean, as demonstrated by *Nakano and Hasumi* [2005]. The model has adjustable, terrain-following, vertical levels. For the model run used in this study, 42 vertical levels are used. Figure B2 illustrates the distribution of the vertical levels along the cross section at 40N. The velocity fields at 1000 m analyzed in section 3 are obtained by a cubic-spline interpolation in the vertical.

Appendix C: Calculation of α Using Simulated Surface Geostrophic Velocity

[37] To show that the behavior of α analyzed in section 3.2 remains similar when the surface velocity is replaced with surface geostrophic velocity, the calculations shown in Figure 5 for the anomalies are repeated for the geostrophic velocity derived from the simulated SSH. Similar to the treatment for the anomalous velocity, the anomaly of the SSH is obtained by removing its long-term mean and the first plus second annual harmonics. The geostrophic velocity is then calculated from the height field anomaly with a fourth-order finite difference scheme. The values of α computed from the geostrophic velocity field are shown in Figure C1 in the same format as Figures 3 and 5.

Appendix D: Increase of α by Temporally Averaging a Rossby Wavefield

[38] As discussed in section 4.2, time averaging can affect the degree of anisotropy of a wavefield if the dispersion relation of the waves is non-isotropic. Quantifying this effect for the ocean is not trivial due to the presence of many different types of waves with different dispersion relations. Just for demonstration, here a simple example is given by considering a random field of only the barotropic Rossby modes with an isotropic spectrum, $|\psi_{\mathbf{k}}|^2 \propto K^{-p}$, where ψ is the barotropic stream function. We use $p = 3$, 3.5, and 4, values that are arbitrarily chosen but partly inspired by the considerations that the globally averaged wave number spectrum for the observed SSH has a slope between -3 and -4 [*Stammer*, 1997]. The contours of constant energy and constant frequency, the latter based on the dispersion relation, $\omega_{\mathbf{k}} = -\beta k_x/(k_x^2 + k_y^2)$, in the wave number plane are illustrated in Figure D1a. For simplicity, we consider a 10,000 km by 10,000 km square domain upon which the wave numbers k_x and k_y are non-dimensionalized. The value of β is held constant using its value at 40N. (The frequency contour plot in Figure D1a is similar to that used by *Vallis and Maltrud* [1993] for a different line of discussion on Rossby wave turbulence. Here, we only use it to illustrate the effect of a linear temporal filter without further implications for the nonlinear dynamics of turbulence.) In Figure D1a, low-pass filtering with a cut-off frequency ω_0 is equivalent to cutting out the shaded area

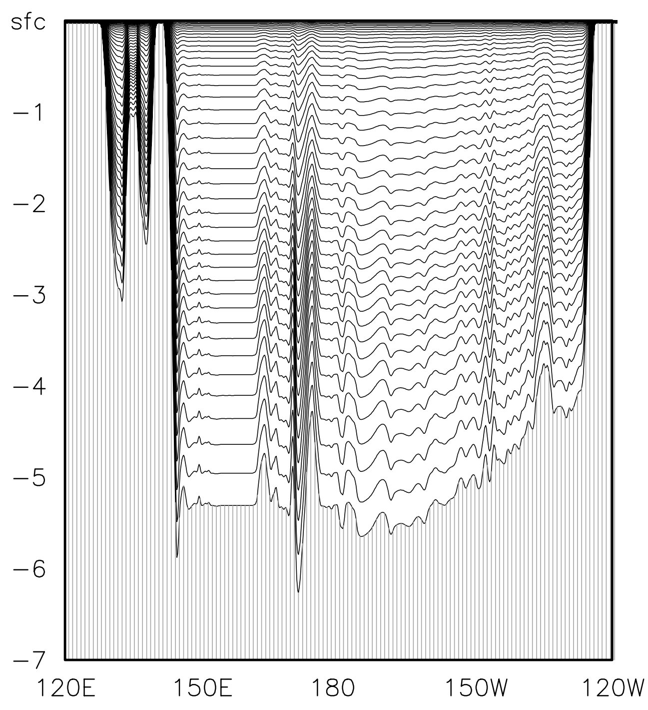

Figure B2. An illustration of the geometry of the terrain-following vertical levels of the model. Shown is the cross section for the North Pacific along 40N. The scales on the ordinate are in km.

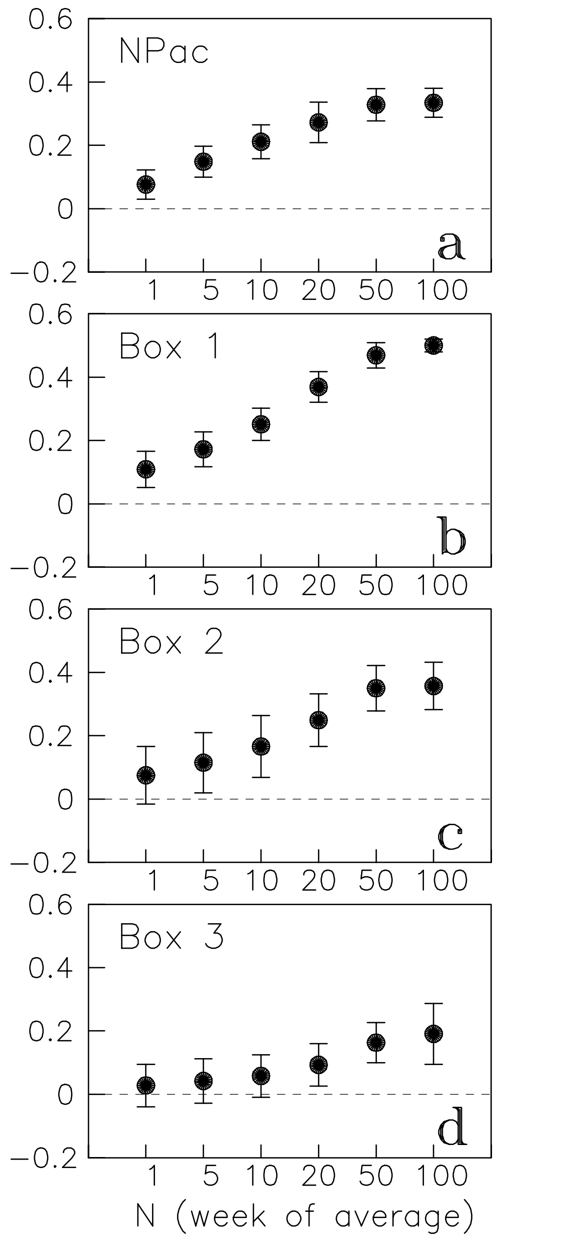

Figure C1. Same as Figure 5 but with α calculated from the surface geostrophic velocity derived from the simulated SSH anomalies.

enclosed by the solid contour for $\omega = \omega_0$. As such, the filter removes meridionally elongated modes (those with $k_x > k_y$) but spares zonally elongated modes, effectively increasing the zonal anisotropy of the flow field.

[39] The values of α for this system as a function of T, the cut-off period (in number of weeks, N) for the low-pass filter, are shown in Figure D1b for p = 3 (black solid), p = 3.5 (black dashed), and p = 4 (black dot-dashed). The calculation of α is done numerically in spectral space with a truncation at total wave number 300. The values of α are somewhat sensitive to the parameter p. Also shown in Figure D1b are two further examples with p = 3 but with the value of β changed to that at 50N (gray dashed) in one case, and with the maximum wave number of spectral truncation changed to 250 (gray solid) in another. Again, they exhibit some sensitivity as the model parameter varies. The observed value of α at the surface for the North Pacific (from Figure 3a) for T = 100 weeks is indicated in Figure D1b as the horizontal dashed line. This is not meant to be a comprehensive comparison but to show that this simple scenario produces values of α that are comparable in magnitude with those observed. The velocity field in the real ocean consists of a much more complicated combination of wave modes (e.g., baroclinic Rossby, gravity) beyond what is considered here. For example, in the situation with a sharp upper-layer stratification, the baroclinic modes may also contributes significantly to the surface stream function [*Smith and Vallis*, 2001; *Scott and Wang*, 2005]. A critical

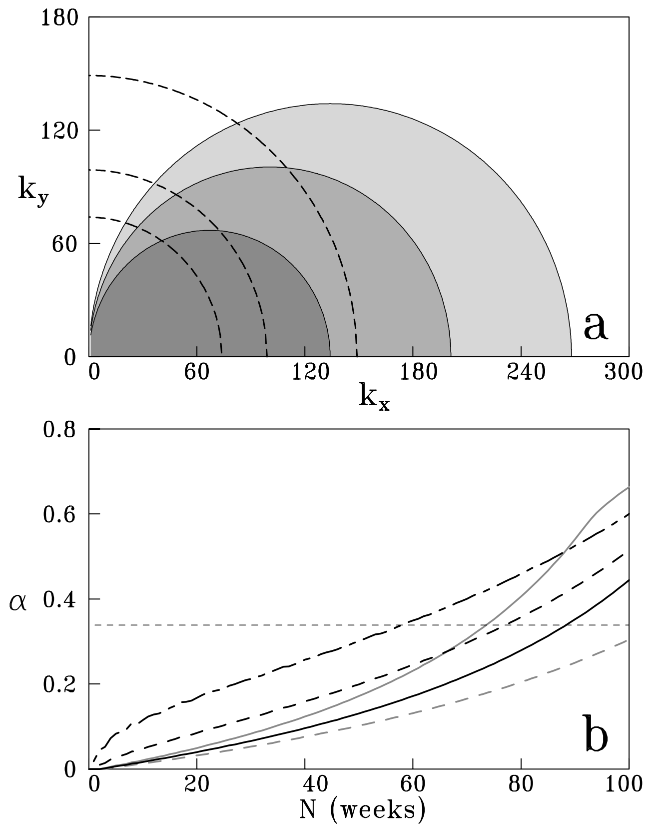

Figure D1. (a) The setup of an idealized scenario for the increase of α with time averaging discussed in Appendix D. The solid curves are contours of constant frequency for the barotropic Rossby mode, with a darker shading corresponding to a higher frequency. The dashed curves are contours of constant energy, and k_x and k_y are zonal and meridional wave numbers. See Appendix D for detail. (b) The change in α with the length of time averaging (in number of weeks, N) for the idealized model for p = 3 (black solid), p = 3.5 (black dashed), and p = 4 (black dot-dashed), all with the value of β for 40N and a spectral truncation at total wave number 300. The two gray curves are the cases with a similar setting as the black solid curve but one with a truncation at K = 250 (solid) and another with the value of β given as that at 50N (dashed). The horizontal dashed line indicates the observed value of α at N = 100 for the North Pacific taken from Figure 3a.

appraisal of the idea presented here must eventually include all major types of waves and vertical modes.

[40] **Acknowledgments.** The authors appreciate the useful comments by two anonymous reviewers that helped improve the quality of this paper. The work performed by HPH, AK, and EC for this paper was supported in part by the Office of Naval Research, award N00014-05-1-0492. EC was supported by NSF grant OCE 0435592. AK was supported by NASA through membership in its Ocean Surface Topography Science Team. NM was partly supported by NSF grant OCE05-50853, NASA through membership in its Ocean Surface Topography Science Team, and Japan Agency of Marine-Earth Science and Technology (JAMSTEC) through its sponsorship of IPRC. LDEO contribution number 7038. IPRC/SOEST publication number 459/7128. U.S. GLOBEC contribution number 535.

References

Castillo, J. E., J. M. Hyman, M. J. Shashkov, and S. Steinberg (1995), The sensitivity and accuracy of fourth order finite-difference schemes on nonuniform grids in one dimension, *Comput. Math. Applic.*, *30*, 41–55.

Chelton, D. B., and M. G. Schlax (1996), Global observations of oceanic Rossby waves, *Science*, *272*, 234–238.

Chelton, D. B., R. A. deSzoeke, M. G. Schlax, K. El Naggar, and N. Siwertz (1998), Geographical variability of the first-baroclinic Rossby radius of deformation, *J. Phys. Oceanogr.*, *28*, 433–460.

Chelton, D. B., M. G. Schlax, R. M. Samelson, and R. A. deSzoeke (2006), Global observations of westward energy propagation in the ocean: Rossby waves or nonlinear eddies?, *Eos Trans. AGU*, *87*(52), Fall Meet. Suppl., Abstract OS13E-07.

Cox, M. D. (1987), An eddy-resolving numerical model of the ventilated thermocline: time dependence, *J. Phys. Oceanogr.*, *17*, 1044–1056.

Curchitser, E. N., D. B. Haidvogel, A. J. Hermann, E. L. Dobbins, T. M. Powell, and A. Kaplan (2005), Multi-scale modeling of the North Pacific Ocean: Assessment and analysis of simulated basin-scale variability (1996–2003), *J. Geophys. Res.*, *110*, C11021, doi:10.1029/2005JC002902.

Ducet, N., P. Y. LeTraon, and G. Reverdin (2000), Global high-resolution mapping of ocean circulation from TOPEX/Poseidon and ERS-1 and -2, *J. Geophys. Res.*, *105*, 19,477–19,498.

Fu, L.-L., and G. R. Flierl (1980), Nonlinear energy and enstrophy transfers in a realistically stratified ocean, *Dyn. Atmos. Oceans*, *4*, 219–246.

Galperin, B., H. Nakano, H.-P. Huang, and S. Sukoriansky (2004), The ubiquitous zonal jets in the atmospheres of giant planets and Earth's oceans, *Geophys. Res. Lett.*, *31*, L13303, doi:10.1029/2004GL019691.

Huang, H.-P., B. Galperin, and S. Sukoriansky (2001), Anisotropic spectra in two-dimensional turbulence on the surface of a rotating sphere, *Phys. Fluids*, *13*, 225–240.

Jayne, S. R. (2006), The circulation of the North Atlantic Ocean from altimetry and the Gravity Recovery and Climate Experiment geoid, *J. Geophys. Res.*, *111*, C03005, doi:10.1029/2005JC003128.

Large, W. G., and S. Yeager (2004), Diurnal to decadal global forcing for ocean and sea-ice models: the data sets and flux climatologies, NCAR Tech. Note TN-460+STR, 105 pp.

Logan, L., R. B. Scott, B. K. Arbic, C. L. Holland, A. Sen, and B. Qiu (2006), Persistent, patchy, and robust small-scale anisotropy in the upper ocean: A fundamental shift in our view of geostrophic turbulence, *Eos Trans. AGU*, *87*(52), Fall Meet. Suppl., Abstract OS11B-1487.

Maximenko, N. A., and P. P. Niiler (2005), Hybrid decade-mean global sea level with mesoscale resolution, in *Recent advances in marine science and technology, 2004*, N. Saxena (Ed.), pp. 55–59, PACON, Honolulu.

Maximenko, N. A., and P. P. Niiler (2006), Zonal jets standing in the meridional geostrophic flow, *Eos Trans. AGU*, *87*(52), Fall Meet. Suppl., Abstract OS11B-1489.

Maximenko, N. A., B. Bang, and H. Sasaki (2005), Observational evidence of alternating zonal jets in the world ocean, *Geophys. Res. Lett.*, *32*, L12607, doi:10.1029/2005GL022728.

Morrow, R., F. Birol, D. Griffin, and J. Sudre (2004), Divergent pathways of cyclonic and anti-cyclonic ocean eddies, *Geophys. Res. Lett.*, *31*, L24311, doi:10.1029/2004GL020974.

Nakano, H., and H. Hasumi (2005), A series of zonal jets embedded in the broad zonal flows in the Pacific obtained in eddy-permitting ocean general circulation models, *J. Phys. Oceanogr.*, *35*, 474–488.

Pascual, A., Y. Faugère, G. Larnicol, and P.-Y. Le Traon (2006), Improved description of the ocean mesoscale variability by combining four satellite altimeters, *Geophys. Res. Lett.*, *33*, L02611, doi:10.1029/2005GL024633.

Rhines, P. B. (1975), Waves and turbulence on a beta-plane, *J. Fluid Mech.*, *69*, 417–443.

Rhines, P. B. (1979), Geostrophic turbulence, *Ann. Rev. Fluid Mech.*, *11*, 404–441.

Richards, K. J., N. A. Maximenko, F. O. Bryan, and H. Sasaki (2006), Zonal jets in the Pacific Ocean, *Geophys. Res. Lett.*, *33*, L03605, doi:10.1029/2005GL024645.

Scott, R. B., and F. Wang (2005), Direct evidence of an oceanic inverse kinetic energy cascade from satellite altimetry, *J. Phys. Oceanogr.*, *35*, 1650–1666.

Sen, A., B. K. Arbic, R. B. Scott, C. L. Holland, E. Logan, and B. Qiu (2006), Persistent small-scale features in maps of the anisotropy of ocean surface velocities – implications for mixing?, *Eos Trans. AGU*, *87*(52), Fall Meet. Suppl., Abstract OS13B-1553.

Shchepetkin, A. F., and J. C. McWilliams (2005), The Regional Ocean Modeling System: A split-explicit, free-surface, topography-following coordinate ocean model, *Ocean Modeling*, *4*, 347–404.

Shepherd, T. G. (1990), Isovortical constraints on the statistical-dynamical behaviour of strongly nonlinear two-dimensional and quasi-geostrophic flow, in *Topological Fluid Mechanics*, H. K. Moffatt and A. Tsinober (Eds.), pp. 278–287, Cambridge Univ. Press.

Simmons, A. J., J. W. Wallace, and G. W. Branstator (1983), Barotropic wave propagation and instability, and teleconnection patterns, *J. Atmos. Sci.*, *40*, 1363–1392.

Smith, K. S., and G. K. Vallis (2001), The scales and equilibration of midocean eddies: Freely evolving flow, *J. Phys. Oceanogr.*, *31*, 554–571.

Stammer, D. (1997), Global characteristics of ocean variability estimated from regional TOPEX/POSEIDON altimeter measurements, *J. Phys. Oceanogr.*, *27*, 1743–1769.

Tapley, B. D., D. P. Chambers, S. Bettadpur, and J. C. Ries (2003), Large scale ocean circulation from the GRACE GGM01 geoid, *Geophys. Res. Lett.*, *30*(22), 2163, doi:10.1029/2003GL018622.

Treguier, A. M., N. G. Hogg, M. Maltrud, K. Speer, and V. Thierry (2003), The origin of deep zonal flows in the Brazil Basin, *J. Phys. Oceanogr.*, *33*, 580–599.

Vallis, G. K., and M. E. Maltrud (1993), Generation of mean flows and jets on a beta-plane and over topography, *J. Phys. Oceanogr.*, *23*, 1346–1362.

Wallace, J. M., and N.-C. Lau (1985), On the role of barotropic energy conversions in the general circulation, *Adv. Geophys.*, *28A*, 33–74.

E. N. Curchitser, Institute of Marine and Coastal Sciences, Rutgers University, New Brunswick, NJ 08901, USA. (enrique@marine.rutgers.edu)

H.-P. Huang and A. Kaplan, Lamont-Doherty Earth Observatory of Columbia University, 61 Route 9W, Palisades, NY 10964, USA. (huei@ldeo.columbia.edu; alexeyk@ldeo.columbia.edu)

N. A. Maximenko, International Pacific Research Center, SOEST, University of Hawaii at Manoa, Honolulu, HI 96822, USA. (nikolai@soest.hawaii.edu)